J. Phys. D: Appl. Phys. **46** (2013) 495302 (7pp) doi:10.1088/0022-3727/46/49/495302

Tunable fluorescence from patterned silver nano-island arrays for sensitive sub-cell imaging

Qi Hao[1], Fei Yang[2], Yin Yin[1], Lifang Si[1], Kailin Long[1], Zhongdang Xiao[2], Teng Qiu[1,4] and Paul K Chu[3,4]

[1] Department of Physics and Key Laboratory of MEMS of the Ministry of Education, Southeast University, Nanjing 211189, People's Republic of China
[2] State Key Laboratory of Bioelectronics, School of Biological Science and Medical Engineering, Southeast University, Nanjing 210096, People's Republic of China
[3] Department of Physics and Materials Science, City University of Hong Kong, Tat Chee Avenue, Kowloon, Hong Kong, People's Republic of China

E-mail: tqiu@seu.edu.cn (T Qiu) and paul.chu@cityu.edu.hk (P K Chu)

Received 16 June 2013, in final form 20 September 2013
Published 15 November 2013
Online at stacks.iop.org/JPhysD/46/495302

Abstract
Surface-enhanced fluorescence, a burgeoning technique in biological detection, provides largely enhanced fluorescence signal by exciting localized surfaces plasmons resonance with fluorescent dyes. Nanostructure and surroundings brings great impact on the emission signal, however, insufficient physics about the process limits further improvement on the nanostructure design. In this study, optical properties of Rhodamin-6G molecules on patterned silver nano-island arrays are tailored by precisely controlling the distance between the dyes and silver arrays. The fluorescence signal depends on the distance and the largest enhancement of 10 folds is achieved when the distance is 10 nm. The results are theoretically corroborated by finite difference time domain simulation and applied to cytoskeleton fluorescence imaging using phalloidin–fluorescein isothiocyanate. Our study provides insights into the physical mechanisms associated with the fluorescence enhancement and quenching, and our experiments suggest potential applications to high-sensitivity sub-cell imaging.

(Some figures may appear in colour only in the online journal)

S Online supplementary data available from stacks.iop.org/JPhysD/46/495302/mmedia

1. Introduction

Nanotechnology spurs the development of biological imaging on the heels of the large fluorescence enhancement [1]. Nanoscale metallic particles such as Ag and Au produce strong localized surface plasmon (LSP) resonance in fluorescence and the resulting enhancement factors can be as high as 1000 theoretically [2]. It is possible to tailor the emission by controlling the nanostructure and surroundings in order to achieve high-sensitivity cell imaging [3]. Surface-enhanced cellular imaging has attracted much attention and found potential applications in biomedicine and early cancer detection [4]. However, thorough understanding of the interactions between nanoparticles and fluorescent molecules is still lacking. In systems spanning a single metal nanoparticle to metal aggregates and inhomogeneous metal films, the specific enhancement properties are linked closely to the geometry, thereby making theoretical prediction difficult [5]. One solution is to design repetitive well-defined patterns by for example, electron beam lithography to obtain high-resolution structures [6], but the small sample throughput presents a practical hurdle.

In this work, patterned silver nano-island arrays (PSNAs) are produced on porous anodic alumina (PAA) films. A periodic surface can be fabricated with good reproducibility and controllability with few defects over a wide range and produces the tunable signal required by fluorescence imaging. To avoid silver oxidization and quenching, a dielectric layer is the best solution. In the LSP system, the frequency and intensity are sensitive to the size, size distribution, and

[4] Authors to whom any correspondence should be addressed.

shape of the nanostructures as well as the environment in the vicinity [7, 8]. LSP works only at a very short distance range of no more than 100 nm and is influenced by the dielectric layer. To investigate the quenching and enhancing mechanisms in this process, MgF_2 film is coated on the PSNAs to control the distance between the fluorescent molecules and PSNAs. MgF_2 is chosen for its wide transparent range from ultraviolet to infrared, small refractive index for light extraction, and antibacterial activity [9, 10]. Rhodamine-6G (R6G) molecule, which exhibits good characteristics in surface-enhanced fluorescence, is then spin-coated to study the fluorescence signal [11]. Previous research suggests that surface-enhanced fluorescence is a viable tool for early cancer detection, molecular detection, and cell imaging [1, 11, 12]. However, the effects of the dielectric layer have not been taken into account and there is room for improvement. Our results reveal a distance-dependence phenomenon of the R6G fluorescence signal by studying MgF_2 films with different thickness. Hence, enhancing and quenching occur at the same time. To investigate the mechanism, the local electromagnetic (EM) fields are calculated using the finite difference time domain and to demonstrate the practical significance. This result is applied in cellular fluorescence imaging by coupling PSNAs with phalloidin–fluorescein isothiocyanate (P-FITC) staining on cytoskeleton. By tuning spacing between PSNAs and cells, cytoskeleton fluorescence imaging was significantly improved. It suggests our method has great potential in sub-cell fluorescence imaging.

2. Experimental section

2.1. Preparation of PSNAs

Al foils (99.99% pure) 0.2 mm thick were degreased by acetone and electro-polished in a mixture of ethanol and perchloric acid with volume ratio of 5 : 1 under a constant dc voltage of 15 V for 3 min to further remove surface impurities. After being rinsed in distilled water and drying, the Al foils were anodized separately in a 0.5M oxalic acid solution under a constant dc voltage of 40 V at 10 °C. The Al foils were first anodized for 2 h followed by immersion into a mixture of chromic acid (1.8 wt%) and phosphoric acid (6 wt%) at 75 °C (1 : 1 in volume). After 2 h, the alumina layer that grew at the first step was removed and the surface of the foil became bright. After a second anodizing step for 2 h, the PAA templates were obtained. The PSNAs were obtained by coating silver layer directly onto the PAA template by vacuum thermal evaporation with a vacuum degree of 2.0×10^{-4} Pa and the deposition rate is 0.1 Å s^{-1}. MgF_2 film coating process was followed with the same deposition rate and vacuum degree. The film thickness was controlled to a relative average error of about 5%, shown in figure S1 in the online supplementary data (stacks.iop.org/JPhysD/46/495302/mmedia).

2.2. Cell culture and phalloidin–fluorescein isothiocyanate stain

Mammalian cells (differentiated rat bone mesenchymal stem cells, BMSCs) were used. Stem cells were collected from Sprague–Dawley rats (12-week-old males) and then size-fractionated. All experiments were conducted in accordance with the institutional guidelines for the care and use of experimental animals. Stem cells were cultured in complete medium consisting of α MEM (Invitrogen), 20% fetal bovine serum (FBS; lot-selected for rapid growth of human MSCs, Invitrogen), 100 U ml^{-1} penicillin, 100 μg ml^{-1} streptomycin, and 2mM L-glutamine (Invitrogen) and incubated at 37 °C with 5% CO_2. The cells were cultured for one month and then labelled with P-FITC (Enzo, ALX-350-268-MC01, excitation: 495 nm, emission: 513 nm) to the cytoskeleton protein f-actin. Cells were washed with phosphate buffered saline (PBS). Fixation was performed with 3.7% paraformaldehyde for 10 min at room temperature, followed by incubation in blocking buffer (PBS containing 1% BSA w/v). Cells were stained with a 5 μg ml^{-1} fluorescent phalloidin conjugate solution in PBS for 40 min at room temperature and washed several times with PBS to remove unbound phalloidin conjugate. It is worth noting that P-FITC working solution concentration was diluted to one tenth of its normal concentration to avoid too strong fluorescence emission. Then cells were seeded on standard glass slides and PSNAs templates were put on the monolayer of BMSC cells for fluorescence imaging.

2.3. Instrumentation and data acquisition

Scanning electron microscopy (SEM, FEI Inspect F50) is used to investigate the structures of PSNAs. Atomic force microscopy (Asylum Research MFP-3D AFM) is used to investigate the measurement precision of evaporated film thickness and the uniformity. Spin coating was performed using a single wafer spin processor with a coating rate of 800 rpm for 8 s and then 3000 rpm for 40 s (WS-400E-6NPP-LITE). Vacuum thermal evaporation system (Technol ZHD-400) was used for surface coating. The film thickness was controlled by film-thickness monitor (Taiyao FTM-V). The local EM fields were calculated using commercial finite difference time domain software (RSOFT FULLWAVE). The photoluminescence (PL) spectral analysis was conducted on a Horiba Jobin-Yvon Fluorolog-3 spectrofluorometer. Fluorescence imaging was performed on a Nikon Ti-E inverted microscope equipped with an oil-immersion objective (Apo TIRF 60x, NA 1.49, Nikon). Depending on the fluorophore, exciting was performed with 491 nm laser (Cobolt Calypso) which was reflected into the microscope objective by a dichroic beamsplitter (semrock, R405/488/561/635) and fluorescence emission was filtered by a bandpass filter (semrock, FF01-446/523/600/677) and imaged on an EMCCD camera (Ixon+DU897, Andor). Exposure time was set to 100 ms and fluorescent intensity was calculated by ImageJ for each image.

3. Results and discussion

The fabrication process of PSNAs is schematically illustrated in figure 1. In order to obtain an ordered nanopore array, a two-step anodizing process was adopted [13].

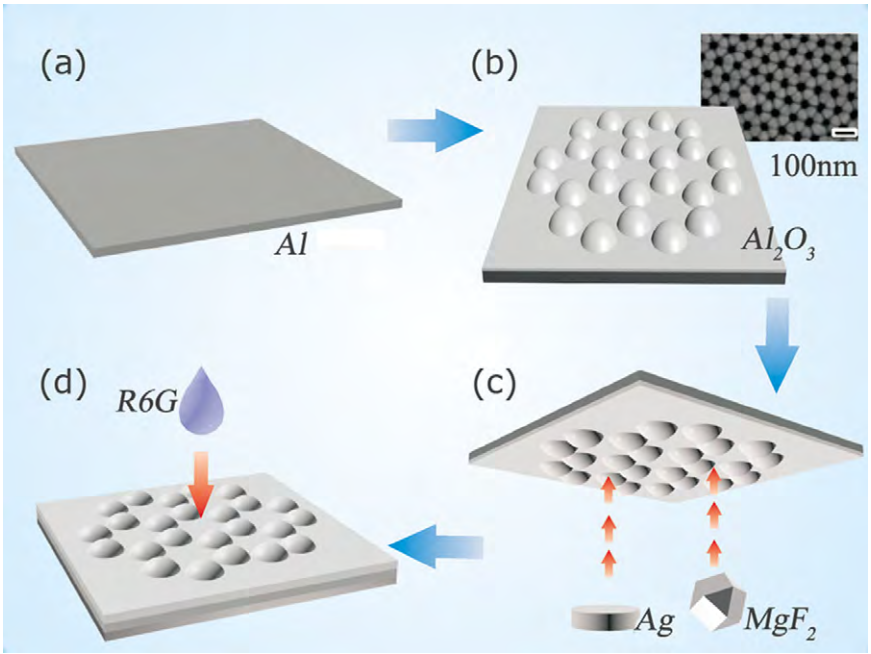

Figure 1. Fabrication process: (*a*) polished aluminum film, (*b*) patterned PAA nanostructure and SEM image, (*c*) surface coating of Ag and MgF_2 by thermal evaporation and (*d*) putting R6G onto the MgF_2 coated PSNAs.

The schematic diagram and typical SEM image of the surface structure (coated with silver for clarity) are shown in figure 1(*b*) and more SEM images with different scale are available in figure S2 in the online supplementary data (stacks.iop.org/JPhysD/46/495302/mmedia). It shows a periodic hexagonal structure with protrusions at the vertex. The space between two protrusions was tailored to 10 nm by optimizing the oxidation time and oxidation voltage. Then silver film was coated on PAA through vacuum thermal evaporation, providing good enhancing effect in visible region and better photostability [14]. The silver layer of 5 nm thick is used for better enhancement (figure S3 in the online supplementary data (stacks.iop.org/JPhysD/46/495302/mmedia)). The silver layer covered the alumina protrusions and the obtained structures had a uniform size of 50 nm and a V-shape dent of 10 nm between two adjacent protrusions due to the similar shape of the alumina protrusions. The V-shape dent provides strong LSP resonance and is ideal for fluorescent molecule absorption [15]. As we know, silver particles are easily oxidized in air and impose negative effects on the fluorescence signals. Besides, direct contact between silver particles and fluorescent molecules causes strong quenching. A dielectric layer seems to be a good solution to protect the sample from quenching and oxidation. Due to the limitation of LSPs, the dielectric layer would strongly affect the enhancement. Previous research has disclosed a distance-dependence phenomenon by adding dielectric layers with different thicknesses between silver and fluorescent molecules [16, 17]. However, there have been no reports on patterned nanoarrays with the LSP system. In our experiments, the MgF_2 layers with different thicknesses of 5, 10, 20, 40 and 60 nm were deposited on the template by vacuum thermal evaporation after silver deposition (figure 1(*c*)). MgF_2 was chosen in lieu of SiO_2 because MgF_2 is transparent in a wide wavelength range from 120 nm to 8 μm which is beneficial to fluorescence spanning ultraviolet and IR. Besides, MgF_2 has a small refractive index (1.379 at 500 nm) which ought to improve the light extraction efficiency.

The fluorescence signal from R6G on these templates is monitored to determine the best parameters for fluorescence enhancement on PSNAs and explore the underlying mechanism. A drop of 10 μl 1×10^{-5} mol l^{-1} R6G in aqueous solution is spin-coated on the top surface of the PSNAs and a glass slide. Figure 2(*a*) shows the fluorescence data comparing the PL intensity from R6G on PSNAs (right) and corresponding photoluminescence excitation (PLE) of the R6G molecule (left). The position of the PLE peak of R6G is about 525 nm and that of the PL peak is about 560 nm. As mentioned, the V-shape dent on PSNAs is about 10 nm between two adjacent protrusions due to the similar shape of the alumina protrusions. This space is well for providing 'hot spots' for fluorescence enhancement by localizing EM field and inducing plasma resonance [5]. Since the size of R6G is less than 1 nm, it can easily attach to the V-shape dent of the PAA [15] and aggregation can be decreased with the presence of protrusions. In figure 2(*b*) we show R6G signal from PSNAs with subtracted background, silver-coated planar Si surface and glass slide. In the comparison, we define fluorescence intensity of R6G on glass slide as 1X. Results shows fluorescence is enhanced on plane silver surface (1.6X) but not as strong as on PSNAs (2.3X). It shows silver coating and corrugated PSNAs surface both contribute to the fluorescence enhancement. However, enhancement may still come from other sources due to chemical interaction. To reveal the physics involved in this process, MgF_2 film was added to prevent direct contact between the R6G and silver particles. Then enhancement may be inferred to arise from the physical instead of a chemical mechanism. As we know,

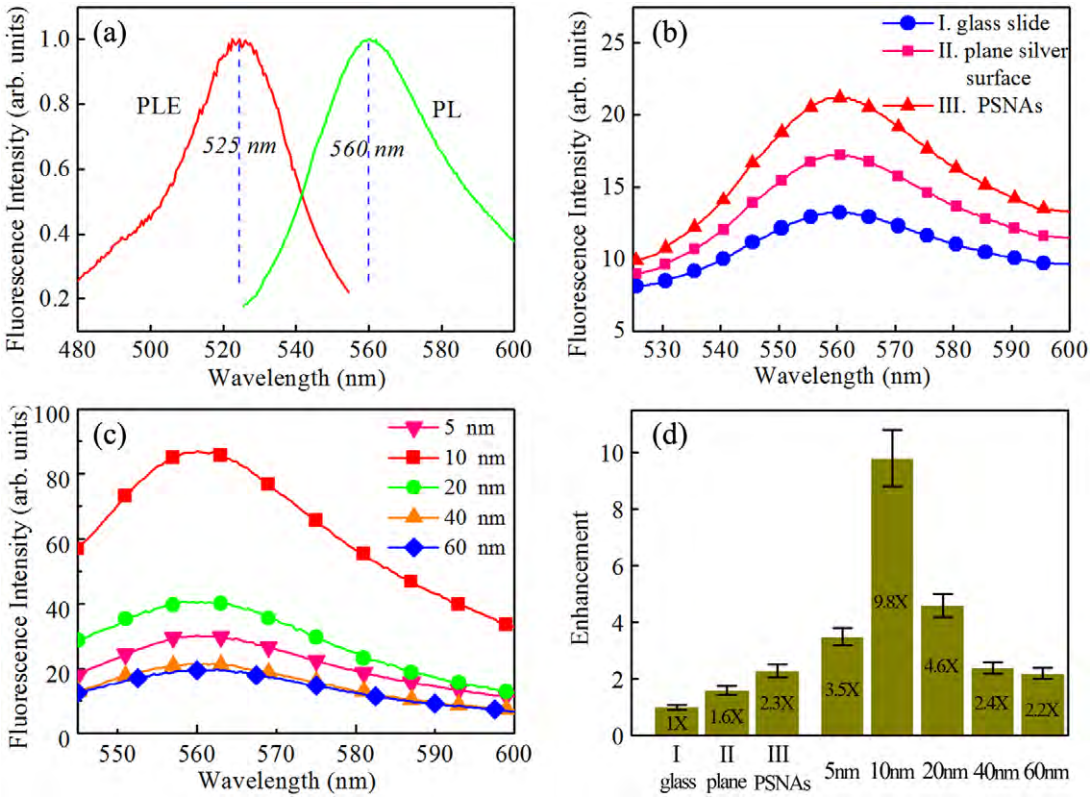

Figure 2. (*a*) PLE, PL spectra of R6G molecules on PSNAs. (*b*) PL spectra of R6G molecules on glass slide, silver-coated plane Si surface and PSNAs. (*c*) PL spectra of R6G with different distances of 5nm, 10 nm, 20 nm, 40 nm and 60 nm from PSNAs, respectively. (*d*) Enhancement factor of fluorescence from samples in (*b*) and (*c*).

EM field decays rapidly with increasing distance. However, a small plasmon exciton spacing (<10 nm) with strong EM field causes unavoidable quenching [18]. Hence, in order to enhance the emission, the spacing has to be finely tuned. The PL intensity of R6G on a series of silver-coated PAA substrates with different MgF_2 film thicknesses between 5 and 60 nm is monitored (figure 2(*c*)). The enhancement factor is calculated and recorded in figure 2(*d*). An obvious distance-dependence phenomenon is observed and the fluorescence intensities vary with increasing spacings between the R6G and silver particles. The strongest enhancement of 9.8 folds relative to glass slide is achieved when the spacing is 10 nm. The enhancement factors are 3.5, 9.8, 4.6, 2.4 and 2.2 for spacings of 5 nm, 10 nm, 20 nm, 40 nm and 60 nm, respectively. When the spacing is larger than 10 nm, the PL intensity diminishes with increasing distance, but below 10 nm, the fluorescence signal is also weaker possibly due to the combined action of enhancement and quenching.

There are two possible mechanisms governing the enhancement. The first is surface plasmons excited by the light transferring part of its energy to the fluorophore (R6G). The fluorophore can then radiate producing larger fluorescence intensity. The second mechanism relies on the strong coupling between the excited state of the fluorophore and plasmons. The excited fluorophore can interact with surface plasmon converting part of the fluorophore's non-radiative near-field emission to be radiated by surface plasmons as far-field emission [19]. This process, known as surface plasmon-coupled emission, prevails typically at distances between tens to hundreds nanometres. This process could be confirmed by a reduction in the lifetime of R6G on plasmonic substrates, which has been reported by previous research [11]. The lifetime of a fluorophore in free space is given by

$$\tau_0 = 1/(\Gamma + k_{\mathrm{NR}}), \tag{1}$$

where Γ is the radiative decay rate and k_{NR} is the non-radiative decay rate. Similarly, the quantum yield of a dye in free space can be written as

$$Q_0 = \Gamma/(\Gamma + k_{\mathrm{NR}}). \tag{2}$$

Furthermore, in the presence of a metal nanostructure, the quantum yield Q_{m} and lifetime τ_{m} of the fluorophore are modified to

$$Q_{\mathrm{m}} = (\Gamma + \Gamma_{\mathrm{m}})/(\Gamma + \Gamma_{\mathrm{m}} + k_{\mathrm{NR,m}}) \tag{3}$$

$$\tau_{\mathrm{m}} = 1/(\Gamma + \Gamma_{\mathrm{m}} + k_{\mathrm{NR,m}}). \tag{4}$$

As Q_0 and τ_0 are constant for a given fluorescence dye, a smaller lifetime translates into a larger radiative decay rate and smaller non-radiative decay rate. In addition, a smaller lifetime reduces photobleaching. In the damping process, it occurs at an even shorter distance of usually <10 nm due to strong near-field coupling [5]. Energy is transferred from the excited dipole to the electron–hole pairs of the metal and this energy is ultimately dissipated in the metal resulting in fluorescence quenching. As all of the energy relaxation channels compete

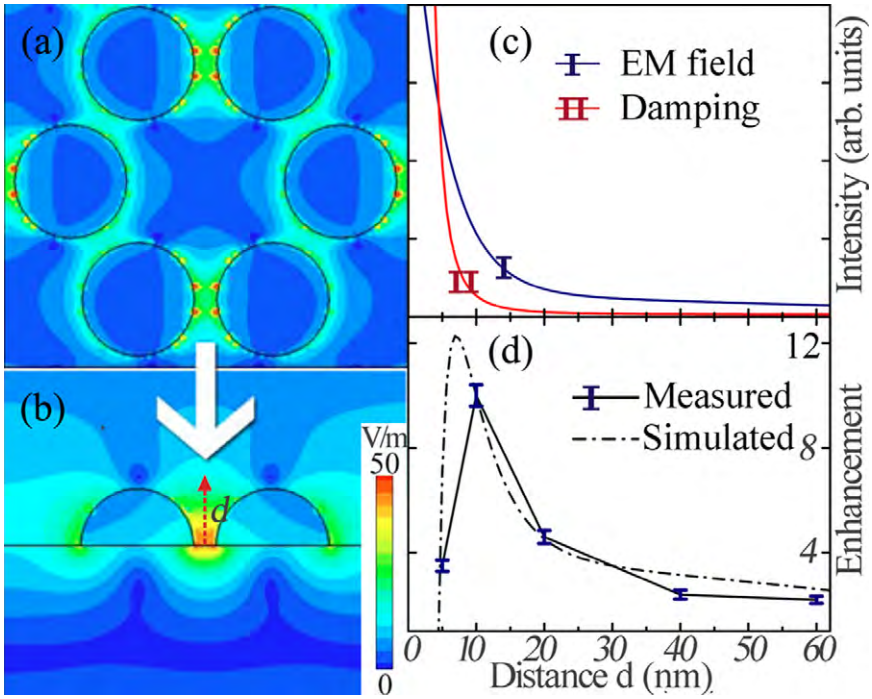

Figure 3. (*a*) Top and (*b*) cross-sectional view of the simulated EM-field distribution maps of PSNAs. (*c*) Damping decay curve and EM-field intensity decay curve. (*d*) Simulated and experimental fluorescence enhancement curves.

with each other, damping becomes the prevailing process for smaller distances even though surface plasmon coupling becomes stronger.

In order to further investigate the enhancement and quenching mechanism, the local EM fields are calculated using the finite difference time domain software. The structure of the PSNAs is approximated by six hexagonally arranged hemispheres using dimensional parameters equal to the mean values of the samples produced experimentally. Light with a wavelength of 500 nm irradiates the sample in the normal direction. Figures 3(*a*) and (*b*) shows the planar and cross-sectional contour plots of the near EM-field distribution showing the maximum local EM field being at the V-shape of PAA. The strongest EM field is located at the V-dent of two protuberances. According to numerical simulations made by Acuna *et al*, a maximum of 117-fold enhancement is available [20]. The EM-field intensity at the centre of the V-shape (showed by the up arrow in figure 3(*b*)) with a distance d and a comparison with the damping rate is shown in figure 3(*c*). The damping curve is determined based on the model suggested by Issa and Guckenberger [21] who reported that the decay rate of the damping process had a d^{-3} dependence. The comparison shows that the damping process plays the leading role when d is less than ∼5 nm and quickly decays to zero after 20 nm. The EM-field intensity diminishes at a relatively smaller rate. Enhancement or quenching is due to the combined effect of these two curves. The difference between the two curves is shown in figure 3(*d*) (dashed–dotted curve) and the experimental data of the R6G enhancement factors with different distances are plotted in figure 3(*d*) (solid line) for comparison. The dashed–dotted curve has a similar shape showing the distance-dependence phenomenon and the simulation and experimental results are consistent. The distance for the strongest enhancement may be less than 10 nm and the relative enhancement factor may be even larger, but it should be noted that the simulation is approximate because other LSPs modes originate from hemispheres not adjacent with other.

Next, we applied our PSNAs in fluorescence cellular imaging by putting PSNAs on the monolayer of BMSCs seeded on glass slide. After the differentiation process, BMSCs showed unique flat structure like a layer of colloidal liquid spreading on the sample surface. This makes it easy for the stained cytoskeleton to get in close touch with PSNAs. The representative confocal images of the P-FITC stained cytoskeletons on PSNAs are depicted in figure 4. A glass slide was used to replace PSNAs for comparison, as shown in figure 4(*e*). All the images were obtained with focus very near to the PSNAs or glass slide. It should be noted the P-FITC solution concentration is 1/10 of that usually used in order to avoid overly bright images. The fluorescence is very strong from the 5 nm thick PSNAs (figure 4(*b*)) but can hardly be observed from the glass slide (figure 4(*e*)). The enhancement factor is calculated and shown in the bar chart by ImageJ software. Data shown here is an average of fluorescence intensity of three different emissive areas in each figure. The intensity of the P-FITC signal on the PSNAs exhibits a distance-dependent phenomenon as aforementioned. The strongest emission from the 5 nm thick PSNAs increases by a factor of 10.4 compared to the glass slide. As the membrane thickness of the cell is about 3–7 nm thick [22, 23], the distance between PSNAs and dyes here should be modified from 5 nm to 8–12 nm. This result shows our PSNAs are good replacements for traditional glass slides. This method could be further developed in intrinsic fluorescence imaging [24] and sensor applications [25].

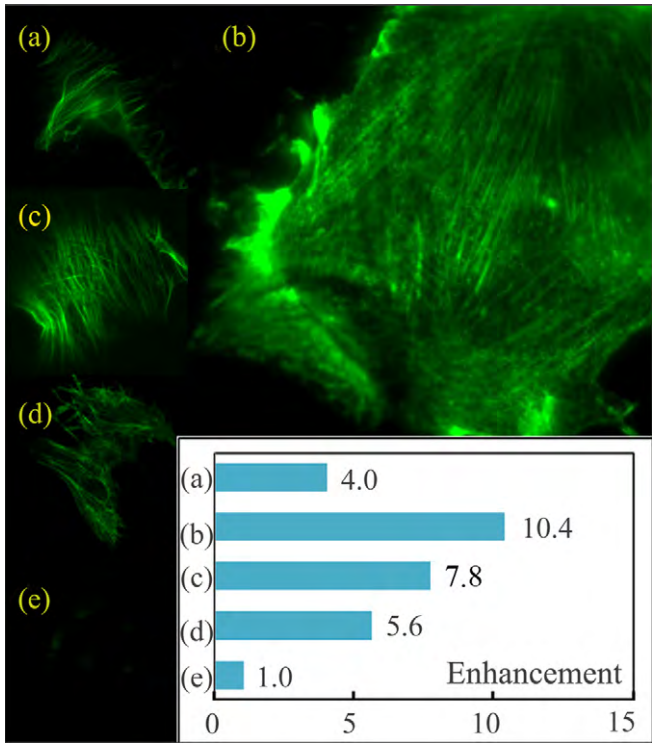

Figure 4. Representative confocal images of cell cytoskeletons labelled with P-FITC on the PSNAs with different MgF_2 thicknesses: (*a*) 0 nm, (*b*) 5 nm, (*c*) 15 nm, (*d*) 35 nm and on glass slide (*e*). P-FITC is excited by the 488 nm laser line. The images are in pseudo colour and the bar chart shows the fluorescence enhancement compared to that on the glass slide.

4. Conclusion

In summary, PSNAs prepared by a simple coating technique on PAA templates are excellent substrates for sub-cell imaging. The fluorescence signals are enhanced significantly by using patterned silver nanostructure and further tuning the distance between the emitter and fluorescence dyes. This enhancement stems from the combined action of damping and enhancing and is confirmed by our experimental and simulation results. The improved emission intensity, smaller lifetime, and better photostability make PSNAs excellent for improving the sensitivity and stability of sub-cell fluorescence imaging. This technique can unveil more subtle details by means of label-free fluorescence detection [26, 27]. Moreover, the low cytotoxicity of silver films compared to quantum dots imaging bodes well for imaging of living cells [28].

Acknowledgments

TQ acknowledges support by the National Natural Science Foundation of China under Grant Nos 51071045 and 51271057, Programme for New Century Excellent Talents in University of Ministry of Education of China under Grant No NCET-11-0096, Natural Science Foundation of Jiangsu Province, China, under Grant No BK2012757, and open research fund of Key Laboratory of MEMS of Ministry of Education, Southeast University. ZDX acknowledges support by the National Basic Research Programme of China (973 Programme: 2013CB932902). PKC acknowledges financial support from Hong Kong Research Grants Council (RGC) General Research Funds (GRF) No CityU 112212 and City University of Hong Kong Applied Research Grants (ARG) No 9667066.

References

[1] Hao Q, Qiu T and Chu P K 2012 Surfaced-enhanced cellular fluorescence imaging *Prog. Surf. Sci.* **87** 23–45
[2] Hutter E and Fendler J H 2004 Exploitation of localized surface plasmon resonance *Adv. Mater.* **16** 1685–706
[3] Zakharko Y, Serdiuk T, Nychyporuk T, Géloën A, Lemiti M and Lysenko V 2012 Plasmon-enhanced photoluminescence of SiC quantum dots for cell imaging applications *Plasmonics* **7** 725–32
[4] Kateb B, Chiu K, Black K L, Yamamoto V, Khalsa B, Ljubimova J Y, Ding H, Patil R, Portilla-Arias J A and Modo M 2011 Nanoplatforms for constructing new approaches to cancer treatment, imaging, and drug delivery: what should be the policy? *Neuroimage* **54** S106–24
[5] Fort E and Grésillon S 2008 Surface enhanced fluorescence *J. Phys. D: Appl. Phys.* **41** 013001
[6] Lin Y, Liu X Q, Wang T, Chen C, Wu H, Liao L and Liu C 2013 Shape-dependent localized surface plasmon enhanced UV-emission from ZnO grown by atomic layer deposition *Nanotechnology* **24** 125705
[7] Garcia M 2011 Surface plasmons in metallic nanoparticles: fundamentals and applications *J. Phys. D: Appl. Phys.* **44** 283001
[8] Hess O, Pendry J, Maier S, Oulton R, Hamm J and Tsakmakidis K 2012 Active nanoplasmonic metamaterials *Nature Mater.* **11** 573–84
[9] Aigueperse J, Mollard P, Devilliers D, Chemla M, Faron R, Romano R and Cuer J P 2005 Fluorine compounds, inorganic *Ullmann's Encyclopedia of Industrial Chemistry* (Weinheim: Wiley)
[10] Lellouche J, Kahana E, Elias S, Gedanken A and Banin E 2009 Antibiofilm activity of nanosized magnesium fluoride *Biomaterials* **30** 5969–78
[11] Gartia M R, Hsiao A, Sivaguru M, Chen Y and Liu G L 2011 Enhanced 3D fluorescence live cell imaging on nanoplasmonic substrate *Nanotechnology* **22** 365203
[12] Qiu T, Jiang J, Zhang W, Lang X, Yu X and Chu P K 2010 High-sensitivity and stable cellular fluorescence imaging by patterned silver nanocap arrays *ACS Appl. Mater. Interfaces* **2** 2465–70
[13] O'sullivan J P and Wood G C 1970 The morphology and mechanism of formation of porous anodic films on aluminium *Proc. R. Soc. Lond.* A 511–43
[14] Le Guével X, Trouillet V, Spies C, Li K, Laaksonen T, Auerbach D, Jung G and Schneider M 2012 High photostability and enhanced fluorescence of gold nanoclusters by silver doping *Nanoscale* **4** 7624–31
[15] Qiu T, Kong F, Yu X, Zhang W, Lang X and Chu P K 2009 Tailoring light emission properties of organic emitter by coupling to resonance-tuned silver nanoantenna arrays *Appl. Phys. Lett.* **95** 213104
[16] Gryczynski I, Malicka J, Nowaczyk K, Gryczynski Z and Lakowicz J R 2004 Effects of sample thickness on the optical properties of surface plasmon-coupled emission *J. Phys. Chem.* B **108** 12073–83
[17] Ray K, Badugu R and Lakowicz J R 2007 Polyelectrolyte layer-by-layer assembly to control the distance between fluorophores and plasmonic nanostructures *Chem. Mater.* **19** 5902–9
[18] Bardhan R, Grady N K, Cole J R, Joshi A and Halas N J 2009 Fluorescence enhancement by Au nanostructures: nanoshells and nanorods *Acs Nano* **3** 744–52

[19] Isfort G, Schierbaum K and Zerulla D 2006 Causality of surface plasmon polariton emission processes *Phys. Rev.* B **73** 033408
[20] Acuna G, Möller F, Holzmeister P, Beater S, Lalkens B and Tinnefeld P 2012 Fluorescence enhancement at docking sites of DNA-directed self-assembled nanoantennas *Science* **338** 506–10
[21] Issa N A and Guckenberger R 2007 Fluorescence near metal tips: The roles of energy transfer and surface plasmon polaritons *Opt. Express* **15** 12131–44
[22] Alberts B, Johnson A, Lewis J, Raff M, Roberts K and Walter P 2002 *Molecular Biology of the Cell* (New York: Garland Science)
[23] Chen A and Moy V T 2000 Cross-linking of cell surface receptors enhances cooperativity of molecular adhesion *Biophys. J.* **78** 2814–20
[24] Akbay N, Lakowicz J R and Ray K 2012 Distance-dependent intrinsic fluorescence of proteins on aluminum nanostructures *Proc. SPIE* (Plasmonics in Biology and Medicine IX) pp 823417–8
[25] Doria G, Conde J, Veigas B, Giestas L, Almeida C, Assunção M, Rosa J and Baptista P V 2012 Noble metal nanoparticles for biosensing applications *Sensors* **12** 1657–87
[26] Cinel N A, Bütün S and Özbay E 2012 Electron beam lithography designed silver nano-disks used as label free nano-biosensors based on localized surface plasmon resonance *Opt. Express* **20** 2587–97
[27] Ali M, Hashim U, Mustafa S, Man Y C, Yusop M, Bari M, Islam K N and Hasan M 2011 Nanoparticle sensor for label free detection of swine DNA in mixed biological samples *Nanotechnology* **22** 195503
[28] Maysinger D, Behrendt M, Lalancette-Hébert M and Kriz J 2007 Real-time imaging of astrocyte response to quantum dots: in vivo screening model system for biocompatibility of nanoparticles *Nano Lett.* **7** 2513–20

Supplementary data

Tunable fluorescence from patterned silver nano-island arrays for sensitive sub-cell imaging

Qi Hao[1], Fei Yang[2], Yin Yin[1], Lifang Si[1], Kailin Long[1], Zhongdang Xiao[2], Teng Qiu[1,4], and Paul K. Chu[3,4]

[1]Department of Physics and Key Laboratory of MEMS of the Ministry of Education, Southeast University, Nanjing 211189, P. R. China

[2]State Key Laboratory of Bioelectronics, School of Biological Science and Medical Engineering, Southeast University, Nanjing 210096, P. R. China

[3]Department of Physics and Materials Science, City University of Hong Kong, Tat Chee Avenue, Kowloon, Hong Kong, P. R. China

E-mail: tqiu@seu.edu.cn (T. Qiu) and paul.chu@cityu.edu.hk (P. K. Chu)

[4] Authors to whom any correspondence should be addressed.

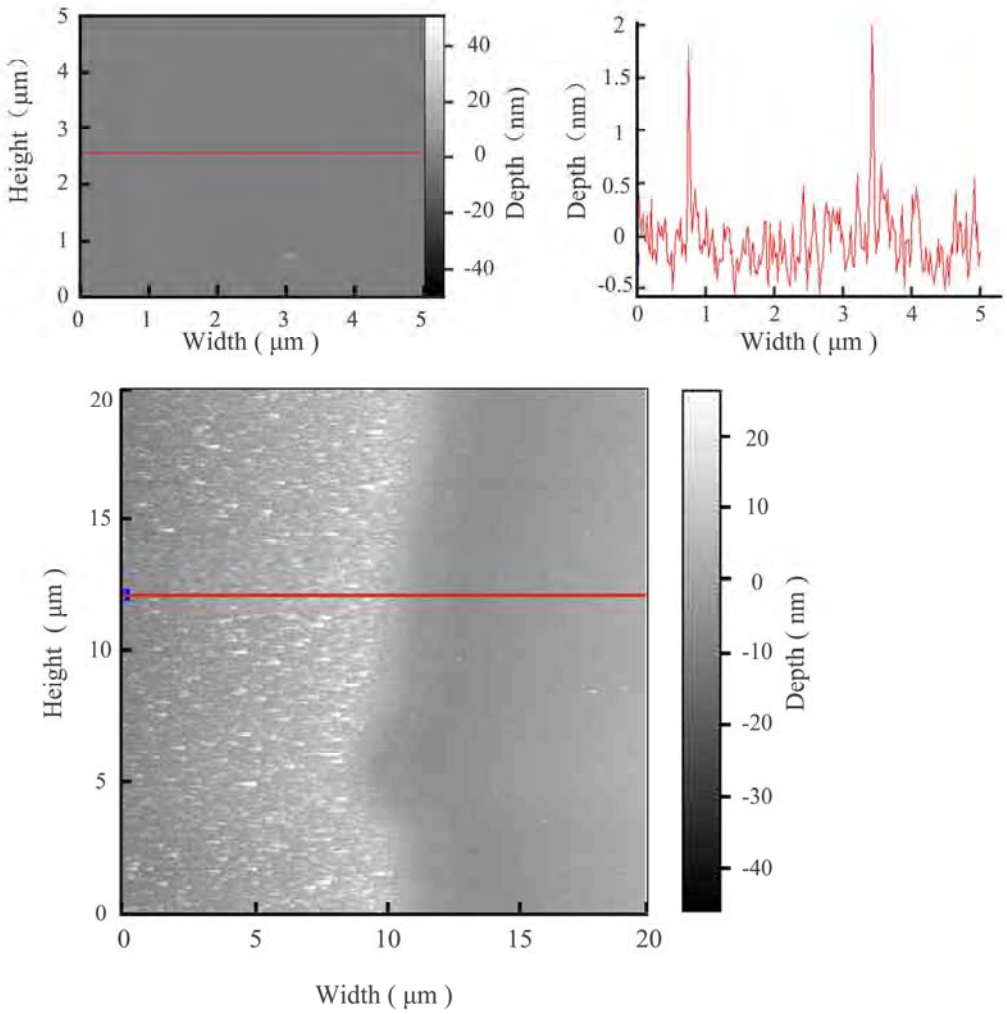

Figure S1. Surface (up) and interfaces (bottom) AFM height retrace roughness data of flat silicon wafers coated with 10nm Ag and 10nm MgF_2. It shows the average deviation surface smoothness of is 1.369 nm and average film thickness is 19.76nm. The abrupt change of film thickness (up) is caused by surface cracks.

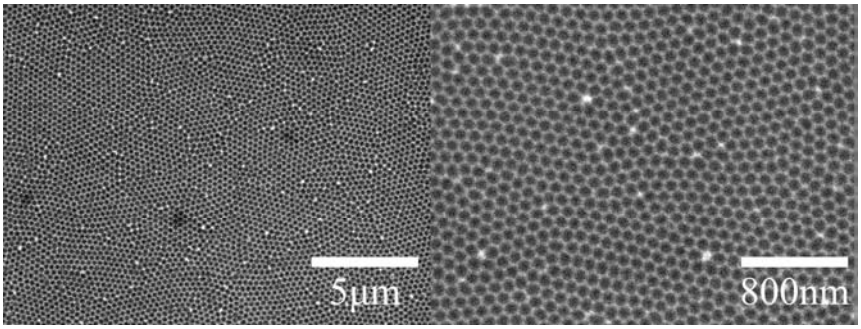

Figure S2. SEM images of PAA substrates.

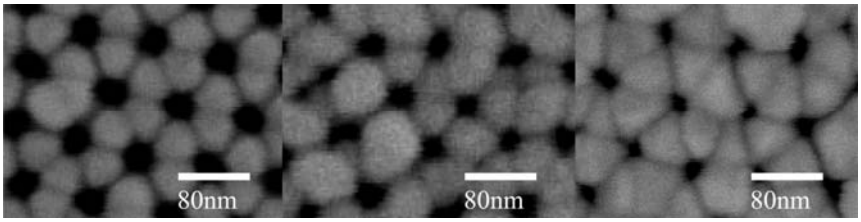

Figure S3. SEM images of PAA substrates coated with silver films. The silver thickness is 5nm, 10nm and 15nm from left to right..